UNIVERSIDADE DE SÃO PAULO

INSTITUTO DE FÍSICA
CAIXA POSTAL 20516
01000 - SÃO PAULO - SP
BRASIL

publicações

IFUSP/P-405

IS QUARK-ANTIQUARK ANNIHILATION INFRARED SAFE AT HIGH ENERGY?

by

J. Frenkel
Instituto de Física, Universidade de São Paulo

J.G.M. Gatheral
Department of Applied Mathematics and Theoretical Physics, University of Cambridge, England

J.C. Taylor
Department of Applied Mathematics and Theoretical Physics, University of Cambridge, England and Instituto de Física, Universidade de São Paulo

Maio/1983

IS QUARK-ANTIQUARK ANNIHILATION INFRARED SAFE AT HIGH ENERGY?

J. Frenkel

Instituto de Física, Universidade de São Paulo, Brasil

J.G.M. Gatheral

Department of Applied Mathematics and Theoretical Physics,
University of Cambridge, England

J.C. Taylor

Department of Applied Mathematics and Theoretical Physics,
University of Cambridge, England

and

Instituto de Física, Universidade de São Paulo, Brasil

ABSTRACT

In perturbative QCD, the Bloch-Nordsieck cross-section for quark-antiquark annihilation is known, to order g^4, to be infrared finite, except for terms which are power-suppressed at high energies. We give a fairly simple explanation of this fact, using analyticity, unitarity and an analysis of mass-singularities in both Feynman and axial gauges. The argument applies fairly easily to order g^6. Assuming a generalized unitarity principle, the argument can be extended to all orders.

1. INTRODUCTION

Can the methods of perturbative QCD be used to calculate the Drell-Yan cross-section by relating it to the cross-section for quark-antiquark annihilation? A necessary condition is probably that the latter should be rendered free of soft divergences by Bloch-Nordsieck cancellation. For, if this were not the case, interactions with spectator partons would be necessary to cancel the soft divergences, and factorization [1] would fail. This is not obviously a sufficient condition, because there might still be non-factorizing contributions of order 1 from spectators [2]. To order g^4, however, this fear has been shown to be unfounded [3].

In fact, the Bloch-Nordsieck cancellation is known to be incomplete in QCD [4]; but explicit calculation to order g^4 has shown [4] that the uncancelled soft divergences are power-suppressed by a factor $O(m^4/s^2)$. Therefore there is no trouble in practice to leading-twist order.

The question we ask is whether this power-suppression persists to higher orders of perturbation theory. The difficulty in trying to answer this question is that the supression results from cancellation between diagrams with and diagrams without 3-gluon vertices. This is true in the Feynman gauge and the Coulomb gauge and all gauges we have tried. The power-suppression is therefore not a consequence of any general property of individual diagrams, nor is it a simple consequence of gauge-invariance.

We believe that we have identified the reasons for the cancellation in as simple a way as possible. The steps in the argument are, briefly, as follows:

(a) (Section 2). "Gluon-reversal", that is, comparison of the process with soft gluons in the final state with an imagined reaction in which they are in the initial state. The latter is obviously infrared finite, by time-reversal and unitarity.

(b) (Section 4). The eikonal approximation, and an integral representation expressing its scaling properties.

(c) (Section 5). A generalized eikonal exponentiation theorem [5], which allows us to restrict our attention to graphs which are "maximally non-abelian" (MNA).

(d) (Section 6). Simple analytic properties of the integral representation in (b), assuming a smooth limit as $m^2/s \to 0$.

(e) (Section 7). Using (a) and (d), cancellation up to $O(m^2/s)$ of the infrared divergences from simple sets of diagrams (in the Feynman gauge) connected by unitarity.

(f) (Section 8). Analysis of mass-divergences in the axial gauge to show that, in the MNA sector, they cancel in the sum of all diagrams; and so that the assumption in (d) was justified.

One can perhaps see that the argument could not be much simpler than outlined above. For steps (b) and (d), we must use the Feynman gauge, for it is only in this gauge that individual graphs have simple analytic properties. But for step (f), the axial gauge (or possibly some other non-covariant) gauge) is convenient, in order to control the mass-divergences [1].

The theorem in (c) is essential in order to isolate a sector, the MNA sector, in which there are no mass-divergences. Of course, there are mass-divergences in general, and their analysis is essential for the factorization theorems. But

fortunately we can avoid them for the purposes of studying the changes brought about by "gluon-reversal" (a).

In general, the eikonal approximation suffers from unphysical behavior for large transverse-momentum gluons, because the transverse-momentum is not controlled by the eikonal quark denominators. To make physical sense, a transverse-momentum cut-off is probably required, which would complicate the formulae. By isolating the MNA sector, we avoid this problem also.

Any analysis which is claimed to work to all orders of perturbation theory must be treated with some degree of caution. Our application of the generalized unitarity principle in Section 7 supposes that there are no snags in using this property of functions of several complex variables. More seriously, our analysis of mass-singularities in Section 8 assumes that we have correctly traced the physical cause of all mass-singularities from a study of lowest order examples.

Finally, note that we only establish suppression by a factor $O(m^2/s)$. To order g^4, the factor turns out to be $O(m^4/s^2)$ [4]. It is an open question whether this stronger suppression occurs at higher orders.

2. GLUON REVERSAL

The first step in our argument is to compare the probabilities for

$$q(p) + \bar{q}(p') \to \gamma^*(Q) + \text{soft gluons}\,(k_1, \ldots k_r) \qquad (2.1)$$

and

$$\gamma^*(Q) \to q(p) + \bar{q}(p') + \text{soft gluons}\,(k_1, \ldots k_r) \qquad (2.2)$$

where q, $\bar{q}$ and γ^* denote quark, antiquark and virtual photon, momenta appear in brackets, and "soft" is defined by

$$|\underset{\sim}{k}_i| < \Delta \qquad (2.3)$$

for each gluon independently. Colours are summed or averaged.

We use the notation

$$2p.k_i = K_i \quad , \quad 2p'.k_i = K'_i \quad , \quad 2k_i.k_j = s_{ij} \, ,$$

$$(p+q)^2 = s \qquad (2.4)$$

and we assume that

$$\Delta^2 \ll s \quad , \quad s_{ij} \ll K_k, K'_\ell \ll s \qquad (2.5)$$

so that

$$Q^2 \approx s \, . \qquad (2.6)$$

The probabilities for the reactions (2.1) and (2.2) can each be written in terms of a single set of quantities F_r, the squared moduli of amplitudes summed over spins and colours (for simplicity, we pretend that the virtual photon is spinless):

$$R(s) = \sum_r \int d^4Q \prod_1^r \frac{d^3k_i}{|\underset{\sim}{k}_i|} \delta^4(p+p'-Q-\textstyle\sum k_i) \times$$

$$\times F_r(s; \gamma, \gamma', \delta; K_i, K'_i; s_{ij}) \, , \qquad (2.7)$$

$$\hat{R}(Q^2) = \sum_r \int \frac{d^3p}{E_p} \frac{d^3p'}{E_{p'}} \prod_i^r \frac{d^3k_i}{|k_i|} \delta^4(p+p'-Q+\sum k_i) \times$$

$$\times F_r(Q^2-\xi-\xi'-\zeta; \xi, \xi', \zeta; -K_i, -K_i'; s_{ij}) \tag{2.8}$$

where

$$\xi = 2p\cdot q \qquad \xi' = 2p'\cdot q \qquad , \quad \zeta = q^2 \ ,$$

$$q = Q - p - p' \tag{2.9}$$

In (2.7) and (2.8), the k_i-integrations are each bounded by (2.3), and the Q, p and p'-integrations are over small regions $q \approx 0$.

We wish to express the phase-space integrals in (2.7) and (2.8) in terms of invariants. To this end, we define

$$H_\pm(s; \xi, \xi', \zeta) = \sum_r \int \prod_i^r \frac{d^3k_i}{|k_i|} \delta^4(q \pm \sum k_i) \times$$

$$\times F_r(s; \xi, \xi', \zeta; \pm K_i, \pm K_i'; s_{ij}) \tag{2.10}$$

Then

$$R(s) = \tfrac{1}{2}\pi \left[s(s-4m^2)\right]^{-1/2} \int d\xi\, d\xi'\, d\zeta\, H_+(s; \xi, \xi', \zeta) \ , \tag{2.11}$$

$$\hat{R}(Q^2) = \pi^2 (Q^2)^{-1} \int d\xi\, d\xi'\, d\zeta\, H_-(Q^2-\xi-\xi'-\zeta; \xi, \xi', \zeta) \tag{2.12}$$

Since

$$\xi + \xi' + \zeta = O(k_i)$$

we can, up to infrared convergent terms, replace (2.12) by

$$\hat{R}(Q) \approx \pi^2 (Q^2)^{-1} \int d\xi\, d\xi'\, d\zeta\, H_-(Q^2; \xi, \xi', \zeta) \tag{2.13}$$

The integrations in (2.11), (2.12) and (2.13) are over small regions, with $\xi, \xi' \le 0$ in (2.11) and $\xi, \xi' \ge 0$ in (2.12) and (2.13).

A unitarity argument [6] assures that $\hat{R}(Q^2)$ is infrared finite. (For a contrary opinion, see [7].) In order to find the infrared properties of $R(s)$, it is therefore sufficient to study the quantity

$$H_+(s; \xi, \xi', \zeta) - H_-(s; -\xi, -\xi', \zeta) \ . \tag{2.14}$$

In subsequent section, we will be concerned with the infrared properties of this quantity.

In the above equations, we have not been precise about the regions of integration. If we were concerned to calculate non-vanishing and non-leading this would matter. Since we only want to show that there are no infrared divergences (up to $O(m^2/s)$), we believe this imprecision is unimportant.

3. HARD AND SOFT GLUONS

In our proof of infrared finiteness (up to $O(m^2/s)$), we adopt a strategy formulated for instance in reference [8]. We divide each gluon integration (real or virtual) into two

regions, $|\underset{\sim}{k}| < \Delta$ and $|\underset{\sim}{k}| > \Delta$. (The k_o-integration for a virtual gluon is unrestricted).

We proceed inductively, and assume that infrared finiteness has been proved up to and including order $g^{2(N-1)}$. Suppose, to order g^{2N}, we encounter an infrared divergent graph, some of its gluons having $|\underset{\sim}{k}| < \Delta$ and perhaps some having $|\underset{\sim}{k}| > \Delta$. The gluons contributing to the infrared divergence must be attached to external quark lines (directly or via other soft gluons). The gluons with $|\underset{\sim}{k}| > \Delta$ (if any) can none of them be attached to a quark line further out than the innermost soft-gluon vertex. Therefore, the hard-gluons in the graph form a core, whose dependence on the soft-gluon momenta may be neglected (because any power of soft-gluon momenta would render the soft-gluon integrations infrared finite).

Thus the infrared divergence, if any, comes effectively from the soft-gluons, the core being irrelevant. If there was an infrared divergence produced by fewer than N soft-gluons, it would contradict the inductive hypothesis. Therefore, the only possibility we have to consider is that <u>all</u> N gluons to order g^{2N} are soft.

Thus, in principle, all the gluons considered throughout this paper should be soft, with $|\underset{\sim}{k}| < \Delta$. However, for virtual gluons, it is often convenient to extend the region of integration to infinity. We believe that this does not affect the existence of infrared divergences. But we take care to do this only when ultraviolet divergences have been properly renormalized and where the eikonal approximation has not produced unphysical mass-singularities or transverse-momentum divergences. These conditions are satisfied in the MNA sector.

4. <u>THE EIKONAL APPROXIMATION</u>

The eikonal approximation is usually motivated by the argument that, for a soft virtual gluon with momentum k, $k^2 << p.k$, p being a quark momentum. This is not true for gluons with momenta in the transverse direction. We believe that, in general the eikonal approximation is valid for detecting infrared divergences, provided it is used with a cut-off (on the total or transverse three-momentum). It may be dangerous to remove the cut-off in general. We will argue that there is no such danger in the MNA sector.

In this section, we present the eikonal approximation as a way of calculating the leading term for small real gluon momenta. (Purely virtual graphs are irrelevant for (2.14)). We use the Feynman parameter representation for a Feynman integral (in the Feynman gauge). For the purposes of the MNA sector (see Section 5), renormalization is only a small complication (see Appendix A).

Consider a Feynman graph contributing to an amplitude for process (2.1). On the internal gluon lines, let the momenta be ℓ_k and the Feynman parameters be z_k. On the quark (anti-quark) lines, let the momenta be $p+a_i$ $(p'+b_j)$ and the Feynman parameters be $x_i(y_j)$, with $i = 1,\ldots,n$, $j = 1,\ldots,n'$. (Quark loops are of course neglected).

The combined denominator is then

$$D = \sum z_k \ell_k^2 + \sum x_i (2a_i\cdot p + a_i^2) + \sum y_j (2b_j\cdot p' + b_j^2) \qquad (4.1)$$

Momentum conservation at the vertices is expressed by equations

$$\sum_{i\in V} \pm a_i + \sum_{j\in V} \pm b_j + \sum_{k\in V} \pm \ell_k + \sum_{\alpha\in V} k_\alpha = 0 \quad , \qquad (4.2)$$

where $i \in V$ means those quark lines attached to a particular vertex V, etc.. The k_α $(\alpha = 1,\ldots,r)$ are external gluon momenta. The $\pm$ signs apply according as the momenta are out of or into the vertex V.

For given values of the parameters x_i, y_j, z_k, the momenta a_i, b_j, ℓ_k are determined by, in addition to (4.2), the extremum equations (see equation (1.5.27) of reference [9])

$$\sum_{k\in L} \pm z_k \ell_k + \sum_{i\in L} \pm x_i a_i + \sum_{j\in L} \pm y_j b_j + p \sum_{i\in L} \pm x_i + p' \sum_{j\in L} \pm y_j = 0 \qquad (4.3)$$

for each independent closed loop L (the $\pm$ signs depending upon the sense of the momentum in the loop).

The external momenta k_α are assumed small compared to p and p'. We express this by imagining each k_α scaled by a small parameter λ. We look for a self-consistent solution of (4.2) and (4.3) in which

$$x_i, y_j, k_\alpha, a_i, b_j, \ell_k = O(\lambda)$$

$$p, p', z_k = O(1) \qquad (4.4)$$

Then, with neglect of $0(\lambda^2)$, (4.3) becomes

$$\sum_{k\in L} \pm z_k \ell_k + p \sum_{i\in L} \pm x_i + p' \sum_{j\in L} \pm y_j = 0 \qquad (4.5)$$

Similarly, with neglect of $0(\lambda^3)$, (4.1) becomes

$$D = \sum z_k \ell_k^2 + 2p \cdot \sum x_i a_i + 2p' \cdot \sum y_j b_j \qquad (4.6)$$

In terms of D, thus implicitly determined, the Feynman integral takes the form (see equation (1.5.22) of reference [9])

$$\Gamma(\nu - \ell\eta) \int \prod_1^n dx_i \prod_1^{n'} dy_j \prod_1^{\ell+\gamma} dz_k \, \delta(1 - \sum x_i - \sum y_j - \sum z_k) \times$$

$$\times (-D - i\varepsilon E)^{-\nu+\ell\eta} \, E^{\nu-2-(1+\ell)\eta} \, N_{\mu_1\ldots\mu_r} \qquad (4.7)$$

Here E is the determinant factor (called C in [9]) and $N_{\mu_1\ldots\mu_r}$ is the numerator factor. D, E and $N_{\mu_1\ldots\mu_r}$ are each functions of the parameters x_i, y_j, z_k.

The graph is defined to have:

n quark lines

n' antiquark lines

r real gluons

γ 3-gluons vertices (4.8)

$\ell = \frac{1}{2}(n+n'+\gamma-r)$ independent loops

ν = number of propagagors $- 2\ell = \frac{1}{2}(n+n'+\gamma+r)$.

We use dimensional regularization with $d = 4+2\eta$. (These formulae require slight modification for one-particle reducible diagrams).

In the eikonal approximation, defined by (4.4), we neglect x_i, y_j in E and in the δ-function in (4.7). We define

$$x_i = \omega \bar{x}_i \quad , \quad y_j = \omega \bar{y}_j$$

where $$\sum \bar{x}_i + \sum \bar{y}_j = 1 \tag{4.9}$$

Since the only relevant contributions to the integral come from $\omega = 0(\lambda)$, we may extend the range of the ω-integration to $+\infty$, thereby making only an error of relative order λ.

The numerator $N_{\mu_1 \ldots \mu_r}$ is homogeneous in ℓ_k, k_α of degree γ. In the eikonal approximation, $N_{\mu_1 \ldots \mu_r}$ has order λ^γ, and has the form

$$N_{\mu_1 \cdots \mu_r} = \sum_{\tau=0}^{\gamma} \omega^\tau \, N^\tau_{\mu_1 \cdots \mu_r} \tag{4.10}$$

where N^τ is homogeneous in the k_α of order $\gamma - \tau$, and also depends upon p, p', $\bar{x}_i$, $\bar{y}_j$, z_k.

Putting together (4.7), (4.9) and (4.10), we get the integral representation

$$M_{\mu_1 \cdots \mu_r} = \Gamma(\nu - \ell\eta) \sum_\tau \prod d\bar{x}\, d\bar{y}\, dz \; E^{\nu-2-(1+\ell)\eta}_x \times N^\tau_{\mu_1 \cdots \mu_r} \int_0^\infty d\omega \; \omega^{\sigma-1} \left[A\omega^2 + 2B\omega + C - i\varepsilon E\right]^{-\nu+\ell\eta} \tag{4.11}$$

where $$\sigma = n + n' + \tau . \tag{4.12}$$

The quantities A, B and C have the following forms:

$$A = m^2 - s\hat{A} \quad ,$$

$$B = -\sum_{\alpha=1}^{r} B_\alpha \kappa_\alpha - \sum_{\alpha=1}^{r} B'_\alpha \kappa'_\alpha \quad , \tag{4.13}$$

$$C = -\sum_{\alpha,\beta=1}^{r} C_{\alpha\beta} \, s_{\alpha\beta}$$

where $\hat{A}$, B_α, B'_α, $C_{\alpha\beta}$ are each non-negative functions of $\bar{x}_i$, $\bar{y}_j$ and z_k. (These assertions are easily derived from pages 34, 35, 36 of reference [9]).

The ω-integral in (4.11) expresses the scaling properties of the eikonal approximation. It is one of the main tools we will use below.

As an example, we quote the values of A, B and C for the graphs in Fig. 1.

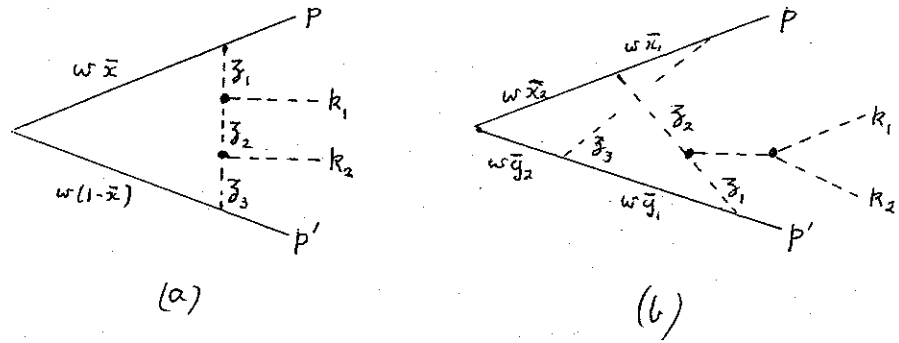

FIG. 1 - Examples of Feynman graphs in the eikonal approximation. Solid lines are quarks or antiquarks and broken lines are gluons. The left hand vertex represents the production from a virtual photon (not shown). Feynman parameters and external momenta are indicated.

For (a), we have

$$A = m^2 - s\bar{x}(1-\bar{x}) \quad ,$$

$$B = -\bar{x}\, p\cdot[(z_2+z_3)k_1 + z_3 k_2] + \\ -(1-\bar{x})\, p'\cdot[z_1 k_1 + (z_1+z_2)k_2] \quad , \qquad (4.14)$$

$$C = -2 z_1 z_3 \, k_1\cdot k_2 \quad ,$$

$$(z_1 + z_2 + z_3 = 1) .$$

We take this opportunity to prove a simple inequality for this graph:

$$B^2 \geqslant \{[\bar{x} z_3 p + (1-\bar{x}) z_1 p']\cdot(k_1+k_2)\}^2$$

$$\geqslant [\bar{x} z_3 p + (1-\bar{x}) z_1 p']^2 (k_1+k_2)^2$$

$$\geqslant 4\bar{x}(1-\bar{x}) z_3 z_1 \, p\cdot p' \, k_1\cdot k_2 > AC \qquad (4.15)$$

In the second step, we have used the fact that k_1, k_2, p and p' are time-like vectors.

The inequality $B^2 > AC$ can be proved for any one-loop graph in essentially the same way.

In the second example, Fig. 1(b), we have

$$A = m^2 - s[z_3\bar{x}_2(\bar{y}_1+\bar{y}_2) + (z_1+z_2)(\bar{x}_1+\bar{x}_2)\bar{y}_2] ,$$

$$B = -\bar{x}_2 z_1 z_3 \, p\cdot(k_1+k_2) - (\bar{y}_1+\bar{y}_2) z_2 z_3 \, p'\cdot(k_1+k_2) ,$$

$$C = -2 z_1 z_2 z_3 \, k_1\cdot k_2 \quad , \qquad (4.16)$$

and the determinant in (4.11) is

$$E = z_3(z_1+z_2) \quad ,$$

$$(z_1+z_2+z_3 = 1 \quad , \quad \bar{x}_1+\bar{x}_2+\bar{y}_1+\bar{y}_2 = 1)$$

We use this example to show that $B^2 \geqslant AC$ is not true in general for multi-loop graphs. To see this, we may for example choose $\bar{x}_1 = \bar{y}_1 = 0$ and

$$k_1 + k_2 = \lambda(z_1\bar{x}_2 p + z_2\bar{y}_2 p') .$$

Then

$$B^2 - AC = \lambda^2 2 p\cdot p' z_1^2 z_2^2 z_3 \bar{x}_2^2 \bar{y}_2^2 (z_3 - 1) + O(m^2).$$

5. GENERALIZED EIKONAL EXPONENTIATION THEOREM

In this section we draw the conclusions which we require from an exponentiation theorem recently proved by one of us [5].

In the present situation, the theorem may be stated as follows. The quantity F_r in (2.7) has the form

$$F_r = \sigma_o\left[\exp\left(\frac{F'}{\sigma_o}\right)\right]_r \qquad (5.1)$$

where F' is defined in the same way as F, but has "maximally non-abelian" (MNA) contributions only, and σ_o is the Born approximation.

The definition of MNA is, roughly, that contributions proportional to

$$g^{2N} C_F C_G^{N-1} \tag{5.2}$$

only are kept, where

$$t_a t_a = C_F 1 \quad , \quad f_{abc} f_{abd} = C_G \delta_{cd} \, . \tag{5.3}$$

Actually, to higher orders, not all colour weights can be expressed in terms of C_F and C_G above. A general, implicit, definition is given in [5].

The notation $[\ ]_r$ in (5.1) means that only contributions to a total number of r real gluons are kept. For example, F_3 has a contribution

$$\frac{1}{3}[\, F_1(\underset{\sim}{k}_1)\, F_2(\underset{\sim}{k}_2, \underset{\sim}{k}_3) + F_1(\underset{\sim}{k}_2)\, F_2(\underset{\sim}{k}_3, \underset{\sim}{k}_1) + F_1(\underset{\sim}{k}_3)\, F_2(\underset{\sim}{k}_1, \underset{\sim}{k}_2)\,]$$

If we write

$$F' = F'_o + F'' \tag{5.4}$$

where F'_o is the purely virtual part of F', we can rewrite (5.1) as

$$F_r = F_o \left[\exp\left(\frac{F''}{\sigma_o} \right) \right]_r \tag{5.5}$$

Since F_o is unaffected by gluon reversal, we need not consider it in (2.14), and we may concentrate on the second term in (5.5).

This has the vital consequence that we may <u>omit</u> from consideration <u>all</u> diagrams with quark self-energy parts, and <u>all</u> diagrams with a vertex part at the quark-antiquark annihilation vertex. These contributions are not MNA, and are contained in the trivial factor F_o.

In the remainder of this paper, we shall refer to all the diagrams in $\sigma_o\, e^{F''/\sigma_o}$ as MNA, not just those in F''.

This result is so important for what follows, we illustrate it with a very simple example. Consider the graphs in Fig. 2, and let the corresponding contributions to F be

$$C_F F_1^{\,a} \quad , \quad C_F F_o^{\,b} \quad , \quad C_F^2 F_1^{\,c} \, ,$$
$$C_F^2 F_1^{\,d} + C_F C_G F_1^{\,d'} \quad , \quad \sigma_o \tag{5.6}$$

where the colour weights, defined in (5.3), have been displayed. The exponentiation theorem says that, since

$$F_1^{\,c} + F_1^{\,d} = \frac{F_1^{\,a} F_o^{\,b}}{\sigma_o} \tag{5.7}$$

the sum is correctly obtained from terms in

$$\sigma_o \left[\exp\left(\frac{C_F F_o^{\,b}}{\sigma_o} \right) \right] \left[\exp\left(\frac{C_F F_1^{\,c} + C_F C_G F_1^{\,d'}}{\sigma_o} \right) \right] \tag{5.8}$$

Thus we need not consider graph (d) explicitly.

As explained in Section 3, we should consider F defined with a momentum cut-off Δ. However, we believe we can let $\Delta \to \infty$ in the <u>second</u> term on the right-hand side of (5.5) without meeting any difficulties. This is because the MNA sector is free of problems with renormalization (see Appendix A) and free of spurious mass-singularities (see Section 8). This

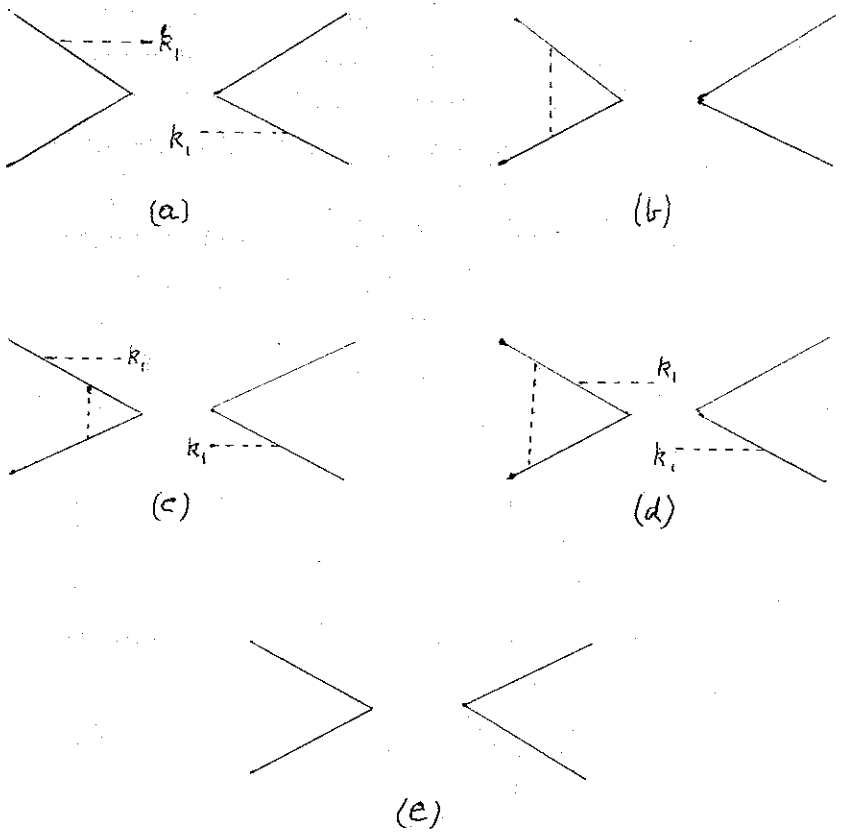

FIG. 2 - Quark-antiquark annihilation graphs contributing to F. The right hand side of each graph represents the complex conjugate of the contribution of which it is the mirror-image. Graph (e) is the Born term, σ_0.

allows us to use the integral representation (4.11), which was derived neglecting any cut-off.

In F_0 in (5.5), the cut-off should probably be retained, but this does not worry us, since we do not have to consider F_0 explicitly in (2.14).

Finally, note that the decomposition (5.5) is gauge-invariant, and is true in any gauge.

6. GLUON REVERSAL AND ANALYTIC PROPERTIES OF EIKONAL AMPLITUDES

In this section, we show how the gluon-reversal transformation from R to $\hat{R}$ in Section 2 is implemented in terms of the integral representation (4.11) for eikonal amplitudes.

Define the amplitude

$$\hat{M}_{\mu_1 \cdots \mu_r}(p, p'; k_\alpha) = (-1)^r M_{\mu_1 \cdots \mu_r}(p, p'; -k_\alpha) \quad (6.1)$$

so that $\hat{R}$ in (2.12) and (2.13) is constructed from $\hat{M}$. The reason for the $(-1)^r$ in (6.1) is that then $\hat{M}=M$ for tree graphs. (We do not consider the case $r=0$ in this section.)

In view of (4.10), (4.11), (4.13) and (6.1), we are lead to compare the integrals

$$I = \int_0^\infty d\omega \; \omega^{\sigma-1} \left[A\omega^2 + 2B\omega + C - i\varepsilon \right]^{-\nu+\ell\eta} \quad (6.2)$$

and

$$\hat{I} = \int_0^{-\infty} d\omega \; \omega^{\sigma-1} \left[A\omega^2 + 2B\omega + C - i\varepsilon \right]^{-\nu+\ell\eta} \quad (6.3)$$

(since the transformation $\omega \to -\omega$ in (6.3) produces a change in sign of B and the $(-1)^r$ in (6.1)).

We shall next study the connection between I and $\hat{I}$. This will turn out to depend crucially upon the sign of A. From (4.13), $A < 0$ except for a region of x_i, y_j, z_k-integration which tends to zero with m^2/s. If the amplitude is well-behaved at $m^2=0$, we could just take the limit $m^2 \to 0$ in (6.2) and (6.3), neglecting terms $O(m^2)$, or, more strictly,

$$O[(m^2)^{1-t\eta}], \tag{6.4}$$

where t is some rational number.

It will emerge in Appendix B that individual graphs have mass-singularities like

$$(m^2)^{\pm \ell\eta} \tag{6.5}$$

at $m=0$, so the naive limit $m^2 \to 0$ cannot be taken. But, we will argue in Section 8, that the singularities (6.5) cancel in a complete set of diagrams in the MNA sector.

We will therefore do as follows. For the remainder of this section we set m^2 small and <u>negative</u> in (4.13), so that $A<0$. We will then deduce an exact relation (6.12) between I and $\hat{I}$. We will then argue that, for a sum of a complete set of MNA graphs, because of the absence of mass singularities, this relation is true up to $0(m^2/s)$ when m^2 is small and positive.

In order to deduce the desired relation, we must study the analytic properties of (6.2). We have to fix the phase of the integrand to define the physical branch of the integral I. This is done by starting in the Euclidean region and continuing with the help of the $i\varepsilon$.

Let

$$f(\omega) \equiv A\omega^2 + 2B\omega + C. \tag{6.6}$$

In the Euclidean region, $A,B,C > 0$ and

$$f^{\ell\eta} = |f|^{\ell\eta} \qquad (0 < \omega < \infty) \tag{6.7}$$

There are branch points at

$$\omega_\pm = A^{-1}\left[-B \pm (B^2 - AC + Ai\varepsilon)^{1/2}\right] \tag{6.8}$$

but these are not on the positive real axis.

Now continue to $A<0$ keeping $B,C>0$. The branch point ω_- moves near the positive real axis and the $i\varepsilon$ dictates that it is below the axis. So

$$\begin{aligned} f^{\ell\eta} &= |f|^{\ell\eta} && , 0 < \omega < \omega_- , \\ &= |f|^{\ell\eta}\, e^{-i\pi\ell\eta} && , \omega_- < \omega < \infty \end{aligned} \tag{6.9}$$

This is shown in diagram (a) of Fig. 3.

Next, continue to $A,C<0$, $B>0$, with $AC<B^2$. The branch point ω_+ moves to a point just above the positive real axis; so

$$\begin{aligned} f^{\ell\eta} &= |f|^{\ell\eta} && , \omega_+ < \omega < \omega_- , \\ &= |f|^{\ell\eta}\, e^{-i\pi\ell\eta} && , \omega_- < \omega < \infty , \\ &= |f|^{\ell\eta}\, e^{-i\pi\ell\eta} && , 0 < \omega < \omega_+ . \end{aligned} \tag{6.10}$$

This is shown in (b) of. Fig. 3.

Finally, we reduce B so that $AC > B^2$. The branch points ω_+ and ω_- move away from the real axis keeping above and below it respectively, as in (c) of Fig. 3. If the cuts are drawn as shown in Fig. 3, we have that

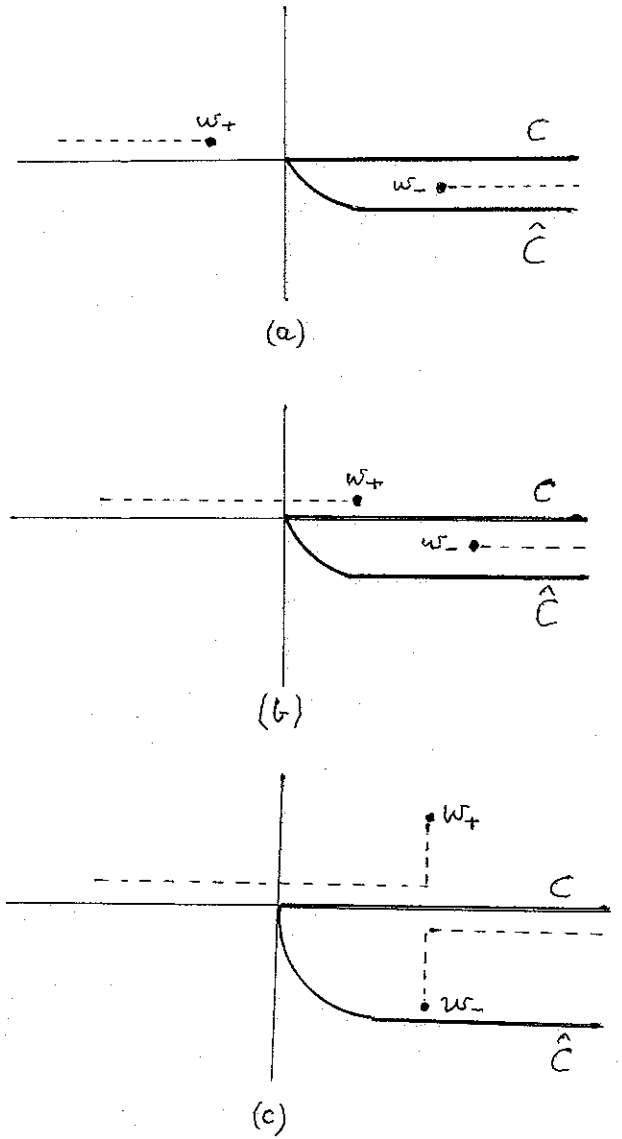

FIG. 3 - The complex ω-plane and the definition of $f^{\ell\eta}$. There are branch points at $\omega_\pm$, and the cuts are drawn as dashed lines. C and $\tilde{C}$ are contours of integration. The three cases are: (a) $A<0$, $B,C>0$; (b) $A,C<0$, $B>0$, $B^2>AC$; (c) $A,C<0$, $B^2<AC$.

$$[f(\omega^*)]^{\ell\eta} = \{[f(\omega)]^{\ell\eta}\}^* \qquad (6.11)$$

in each case.

In Fig. 3, the contour of integration defining the integral I is marked as C. Consider the integral $\tilde{I}$ in (6.3). The contour is along the negative ω-axis (below the ω_+ cut). We may rotate this contour, without passing any singularities, to the positions $\tilde{C}$ shown in Fig. 3.

We next define an integral $\tilde{I}$ to be a non-physical branch of the function I. $\tilde{I}$ is defined by giving all the $s_{\alpha\beta}$ in (4.13) negative imaginary parts, in other words by crossing all the multi-gluon threshold branch cuts (but not altering the other variables, s, K_α, K'_α). Thus $\hat{I}$ is defined by continuing from $C>0$ to $C<0$ with C having a positive imaginary part (but with the previous step from $A>0$ to $A<0$ done as before in Fig. 3(a)).

Thus we start from Fig. 3(a) and give C a positive imaginary part, making the branch-points move into the opposite half-planes from Fig. 3(a). Now, as C is made more and more negative, we get the situations shown in Fig. 4.

Bearing in mind (6.11), we see from Fig. 3 and Fig. 4 that

$$\hat{I} = \tilde{I}^* \qquad (6.12)$$

This is the key relation we wished to derive. It is essential to its derivation that $A<0$, otherwise (6.11) is not true, because $f^{\ell\eta}$ is not real on the real axis between the branch-points (in the diagram corresponding to Fig. 3(b)).

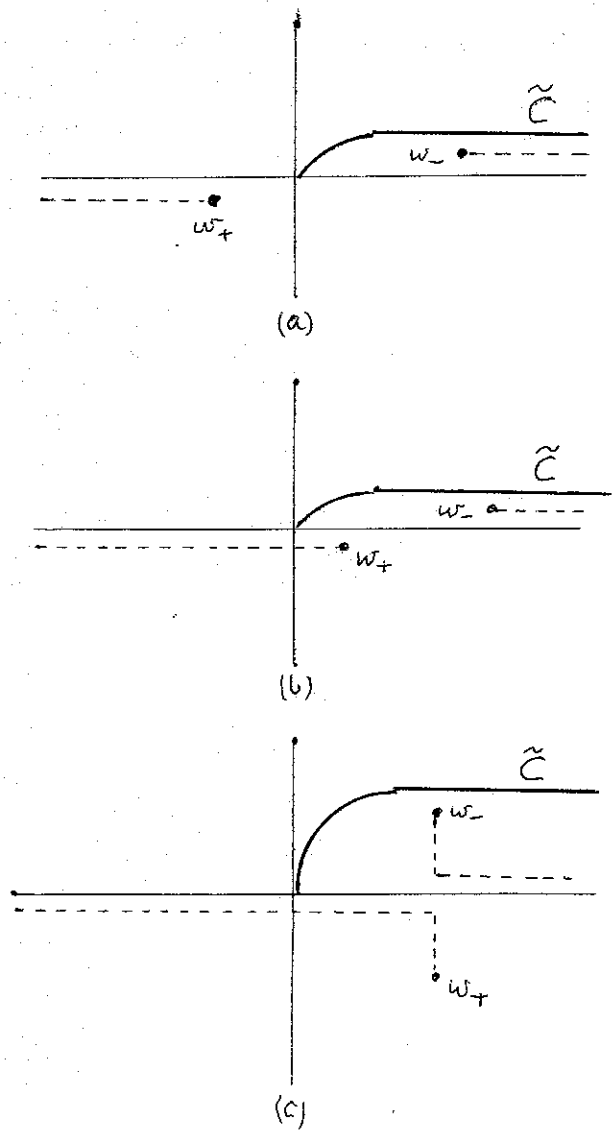

FIG. 4 - The positions of the branch cuts and the contour $\tilde{C}$ defining the unphysical function $\tilde{I}$. The three cases correspond to those in Fig. 3.

We note two special cases of relation (6.12). First, for one-loop diagrams, we have the inequality

$$B^2 > AC \tag{6.13}$$

as shown in the example in (4.15). Then it follows from Fig. 3(b), and equation (6.10) that

$$\hat{I} - I = \left(e^{i\pi\ell\eta} - e^{-i\pi\ell\eta} \right) \times \times \int_{\omega_-}^{\infty} d\omega \;\; \omega^{\sigma-1} \, |f(\omega)|^{-\nu+\ell\eta} \tag{6.14}$$

and so

$$Re\,(\hat{I} - I) = 0 \tag{6.15}$$

Second, for the even more special case when $C \geq 0$ $(A<0)$, Figs. 3(a) and 4(a) show that

$$\tilde{I} - I = 0$$

and so (6.12) becomes

$$\hat{I} = I^* \tag{6.16}$$

For one-particle reducible graphs, the derivation of (6.12) requires a little extra care. This is discussed in Appendix A.

Finally in this section, we repeat that (6.12), (6.15) and (6.16) have been derived under the unphysical assumption that $m^2<0$. In Section 8 we will argue, from the absence of mass singularities like (6.5), that the above equations are valid in the physical region $m^2 \geq 0$ up to terms of order

(6.4). It is in this sense that we shall use (6.12), (6.15) and (6.16) in Section 7:

$$\hat{I} - \tilde{I}^* = O[(m^2)^{1-t\eta}] \quad , \tag{6.17}$$

$$Re(\hat{I} - I) = O[(m^2)^{1-t\eta}] \quad , (B^2 > AC) \quad , \tag{6.18}$$

$$\hat{I} - I^* = O[(m^2)^{1-t\eta}] \quad , \quad (C = 0) \, . \tag{6.19}$$

7. UNITARITY

We next establish from (6.17) that (2.14) is $O\left[(m^2)^{1-t\eta}\right]$. In order to make the argument as persuasive as possible, we begin with the simplest, most special case, and work towards the general case.

To order g^4, $r = 0,1,2$. r=0 means purely virtual virtual diagrams and r=2 means tree diagrams. In either case, (2.14) vanishes trivially. So we may take r=1, which means C=0. The contributions to (2.14) come from products of an order g^3 graph with a (real) order g tree-graph. Therefore (2.14) is of order (6.4) by virtue of (6.18).

Next, consider order g^6. The non-trivial cases are r=1 and r=2. For r=1, one possibility is the product of a g^5 amplitude with a tree-diagram, when again (6.18) may be applied. The other possibility is to have the squared modulus of a g^3 amplitude. Since C=0, this satisfies (6.19), and hence (2.14) is of order (6.4). For r=2, we have g^4 one-loop amplitudes multiplied by (real) tree-graphs; so we may use (6.18), and again (2.14) is of order (6.4).

Next, consider order g^8. A new situation appears for r=2, where we may have a product of two one-loop graphs or the product of a two-loop graph with a tree-graph. Now $C \neq 0$, so the one-loop graphs do not obey (6.19). Also, in general $B^2 \not> AC$, so the two-loop graphs do not obey (6.18). Thus neither type of contribution to (2.14) is of order (6.4) by itself. However, we will show that the two types terms cancel each other.

To see this, write (2.14) in the symbollic form

$$M M^* - \hat{M} \hat{M}^* \quad , \tag{7.1}$$

where a generalized matrix notation is understood including a 2-particle phase-space integral (with $\delta^4(q \pm k_1 \pm k_2)$ as in (2.10)).

Using (6.17), we may re-write (7.1) as (up to order (6.4))

$$M M^* - \tilde{M}^* \tilde{M} =$$

$$= (M - \tilde{M}) M^* + \tilde{M}(M - \tilde{M})^* \tag{7.2}$$

The generalized unitarity principle (see reference [9] equations (4.7.6a) and (4.7.6b)) states that

$$M - \tilde{M} = \tilde{M} S = M \tilde{S} = - M S^* \tag{7.3}$$

where S is the 2-gluon → 2-gluon S-matrix, and again 2-particle phase space integrals are understood. The last form of (7.3) follows from equation (4.2.21b) of reference [9]. Substitution of (7.3) into (7.2) gives

$$\tilde{M} S M^* - \tilde{M} (M S^*)^* = 0 \, , \tag{7.4}$$

as required.

In Fig. 5, we give an example of the structure of a contribution to (7.4). This can arise from (7.2) in two ways, when $M-\tilde{M}$ is $0(g^6)$ and when $(M-\tilde{M})^*$ is $0(g^4)$. The two contributions cancel.

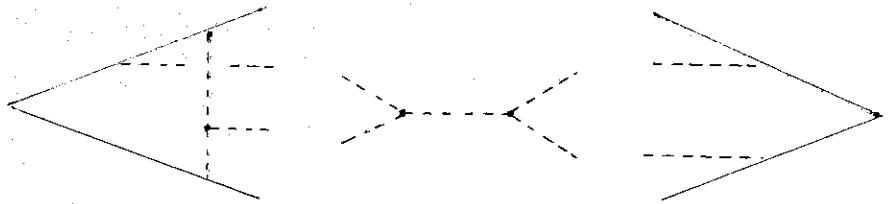

FIG. 5 – Structure of a typical contribution to (7.4) in order g^8. The two left-hand graphs may be a g^6 contribution to $M-\tilde{M}$, and the two right-hand graphs may be a g^4 contribution to $(M-\tilde{M})^*$.

The argument in equations (7.2), (7.3) and (7.4) is now in a completely general form, provided that S is the complete S-matrix in the pure gluon sector. When, say, 3-gluon intermediate states are involved, there are three 2-gluon threshold cuts (in the variables s_{12}, s_{23} and s_{31}), and one 3-gluon threshold cut (in the variables $s_{12}+s_{23}+s_{31}$). The S-matrix includes disconnected pieces depending on single variables s_{12}, s_{23} or s_{31}. Assuming that equations (7.3) generalize, we see no reason why the argument should not apply to all orders.

In this section, we have been dealing with the complete probability function F in (7.1). However, we could equally have restricted ourserlves to the second term in (5.5). This is because the first term, F_0, obeys the trivial equations

$$F_0 = F_0^* = \hat{F}_0$$

and so would factor out of all the equations in this section.

8. MASS-SINGULARITIES AND THE AXIAL-GAUGE

We now consider the behaviour of the integrals in (4.11), (6.2) and (6.3) near $m^2=0$.

For individual diagrams, there are certainly terms behaving like

$$(m^2)^{\pm i\eta} \tag{8.1}$$

as $m^2 \to 0$. This is shown in Appendix C. Such behaviour, if it were uncancelled, would prevent our deducing (6.17) for $m^2>0$ from (6.12) for $m^2<0$.

However, we will argue on quasi-physical grounds, that terms like (8.1) cancel out in a complete set of MNA graphs, leaving terms which differ from a finite limit at $m^2=0$ only by terms

$$O\left[(m^2)^{1-it\eta}\right] \tag{8.2}$$

(t being some rational number). If this is so, we can deduce (6.17), up to this order, from (6.12).

The only known source of "mass-singularities" like (8.1) is collinear configurations of a quark and gluons. Here there are denominators of the form

$$(1-\beta\cos\theta)^{-1}, \tag{8.3}$$

where β is the speed of the (anti-)quark and θ is the angle between the three-momenta of the quark and a gluon. In the centre-of-mass system

$$\beta^2 = 1 - \frac{4m^2}{s} \quad , \tag{8.4}$$

and angular integrals involving (8.3) may give singularities like (8.1) (in dimensional regularization). We give examples in Appendix C.

Next, we take advantage of the gauge-invariance of complete sets of graphs in the eikonal approximation, to repeat the analysis of collinear configurations in the axial gauge [1] (defined by an arbitrary unit space-like vector n_μ). In this gauge, a quark cannot emit a parallel gluon. The matrix element is suppressed by a factor

$$\sin^2\theta \tag{8.5}$$

(more precisely, see equation (D1)). In general, this factor prevents (8.3) from producing mass-singulatiries.

An exception occurs when a gluon is emitted and absorved by the same quark. Then two factors (8.3) can occur, with only one suppression factor (8.5).

The simplest example of this occurs in quark self-energy insertions. However, these are irrelevant in the present context, since such examples are not MNA (or have r=0) (see Section 5). These non-MNA mass-singularities are of vital importance in the factorization theorems [1].

For individual graphs in the axial gauge, mass-singularities can also be generated by graphs or sub-graphs like the examples Fig. 6, in which other gluons ($k_1, k_2, \ldots$) leave

the quark line, in addition to the parallel gluon which is emitted and absorbed. This happens because we are using the eikonal approximation and extending the virtual k-integration to $|k| = \infty$ (see the discussions at the beginning of section 4, and in Appendix D).

However, when a complete set of graphs (like (a)+(b) or (c)+(d)+(e)+...) is added together, the mass-singularities cancel, as we will now demonstrate.

We begin with the lowest order example, graphs (a) and (b) of Fig. 6, and the case when k_1 is a real gluon.

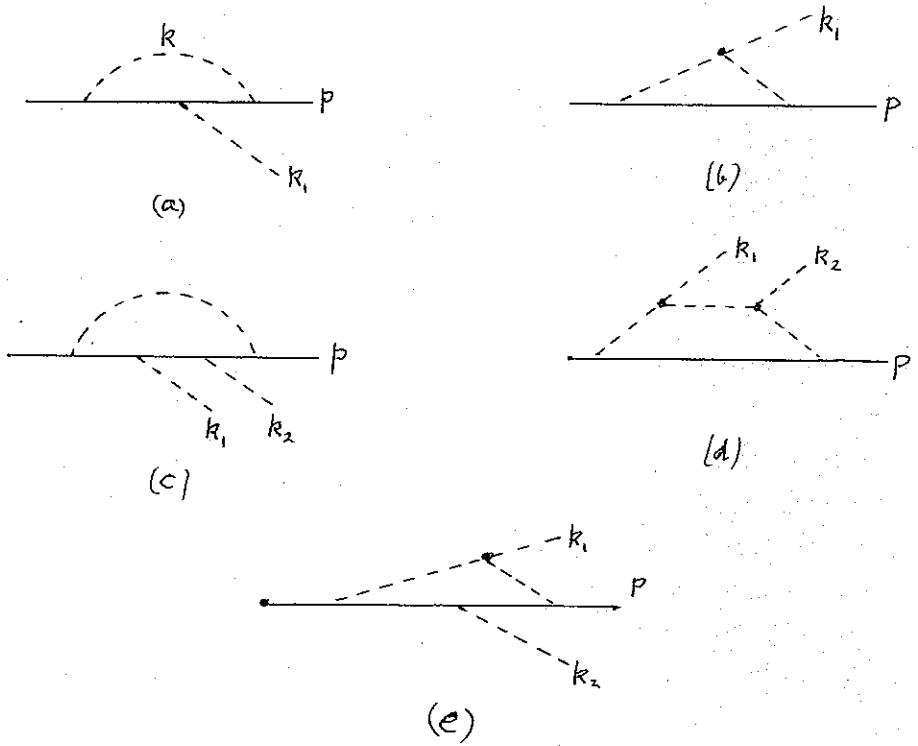

Fig. 6 – Examples of graphs which, individually, in the axial gauge and in the eikonal approximation, give mass-singularities. The singularities cancel when the graphs are added together.

Then, to this order (g^3) in the axial gauge, the only MNA graphs which can possibility give mass-singularities are these two graphs together with the corresponding pair on the p'-line. Therefore, the mass singularity would have to have the form

$$g^3 m^{\pm 2\eta}\left[F_\lambda(p, n, k_1) - F_\lambda(p', n, k_1)\right] \equiv E_\lambda \qquad (8.6)$$

Since this is supposed to be the complete mass-singularity contribution in an S-matrix element, it must be independent of the gauge-vector n_μ. Therefore (8.6) has the form

$$g^3 m^{\pm 2\eta}\left[F_\lambda(p, k_1) - F_\lambda(p', k_1)\right] \quad . \qquad (8.7)$$

By the scaling properties of the eikonal approximation, (8.7) must be

$$g^3\left\{ a\left[\left(\frac{p.k_1}{m}\right)^{2\eta}\frac{p_\lambda}{p.k_1} - \left(\frac{p'.k_1}{m}\right)^{2\eta}\frac{p'_\lambda}{p'.k_1}\right] + \right.$$

$$\left. + b\, k_{1\lambda}\left[\left(\frac{p.k_1}{m}\right)^{2\eta-2} - \left(\frac{p'.k_1}{m}\right)^{2\eta-2}\right]\right\}, \qquad (8.8)$$

where a and b are constants. But, in the axial gauge, the MNA contribution to these graphs, satisfies a simple, homogeneous Ward identity (since there are no ghosts)

$$k_{1\lambda}\, E_\lambda = 0 \qquad (8.9)$$

(in the notation of (8.6)). This implies that

$$a = 0 \qquad (8.10)$$

in (8.8), and hence that there are no mass-singularities (8.1)

in this case.

Next, let us relax the condition that $k_1^2=0$. We argue that his does not alter our conclusion that (8.6) is free of mass-singularities. The reason is, as shown in Appendix D, that the mass-singularity comes from large values of the variable $|\underset{\sim}{k}|$. k_1^2 appears in denominators along with $|\underset{\sim}{k}|$ (not along with $(1-\beta\cos\theta)|\underset{\sim}{k}|$), and so does not alter the behaviour of the integrand for large values of $|\underset{\sim}{k}|$.

Next we extend the argument to two emitted gluons, as in Fig. 6 (c), (d), (e), first assumed to be real. The generalization of (8.8) is

$$g^4 m^{-2\eta}\left[c\, p_\mu p_\nu + c' p'_\mu p'_\nu + O(m^2)\right] \qquad (8.11)$$

where c is a homogeneous function of $p.k_1$ and $p.k_2$ of degree $(2\eta-2)$. The $O(m^2)$ terms include tensors like $p_\mu k_{1\nu}$ whose coefficients are homogeneous of degree $(2\eta-3)$ in $p.k_1$ and $p.k_2$ (like the b-term in (8.8)). The Ward identities got by contracting with k_1^μ or k_2^ν give $c=c'=0$; so again there is no mass-singularity.

The generalization $k_1^2, k_2^2 \neq 0$ is by the same argument as before.

We may now consider two loop graphs. Some examples are shown in Fig. 7. Case (a) is free of mass-divergences by the general argument of equations (8.3) and (8.5). Graphs (b) and (c) are examples where one virtual gluon is emitted and absorbed by the same quark; so they might have had mass-divergences. However, the argument just made about Fig. 6 excludes this possibility.

Thus the only possible mass-divergences occur in graphs like (d) in which all the gluons are attached to one

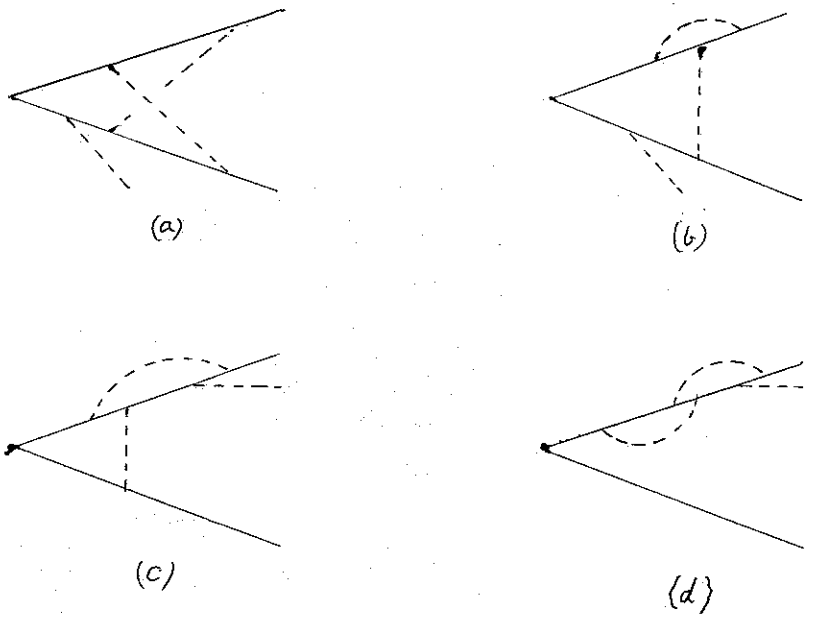

Fig. 7 - Examples of two-loop quarks in the axial gauge. (b) and (c) contain graphs of Fig. 6 as sub.graphs.

quark line. For these graphs, we may repeat the argument involving equation (8.8) (or (8.11)), and show that there are no mass singularities.

We can now go on to graphs with two loops and more real gluons, and then to three-loop graphs. Thus the argument continues inductively.

This completes the argument that mass singularities like (8.1) cancel in the MNA sector in the axial gauge, and therefore in any gauge. This justifies the use of (6.17), (6.18) and (6.19) for $m^2 \geq 0$, and therefore justifies the work of Section 7.

APPENDIX A - RENORMALIZATION IN THE EIKONAL APPROXIMATION

In this Appendix, we want to show by simple examples that one-particle-reducible and ultraviolet divergent graphs make no significant change in the work of Sections 4 and 6. By the argument of Section 5, we may restrict ourselves to the MNA sector. (As explained in Section 3, a cut-off is probably required in order to define F_o in (5.5) properly.)

In the MNA sector, the only ultraviolet divergent sub-graphs are quark-gluon vertex parts and pure-gluon graphs. We give an example of the former, as the pure-gluon graphs are more straightforward. The graphs are given in Fig. 8. We are interested in the MNA part of (a).

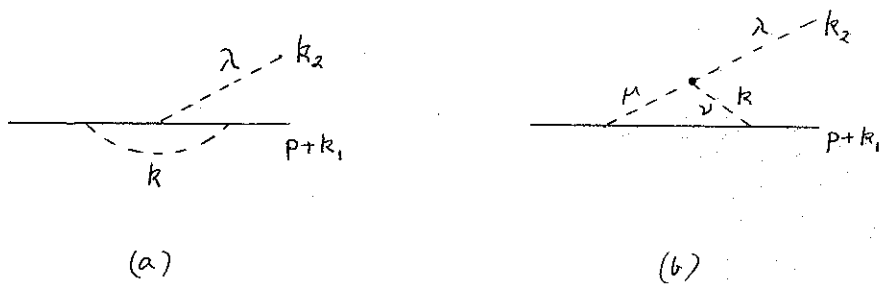

FIG. 8 - Second-order quark-gluon vertex parts.

Let us first take the contribution V_λ^a from (a) (with the C_G colour weight) and the contribution V_λ^b from (b) which comes from the

$$g_{\mu\nu}(2k + k_2)_\lambda \qquad \text{(A1)}$$

term in the 3-gluon vertex. The divergent parts of the integrals are, apart from uninteresting factors,

$$V_\lambda^a = 2m^2 p_\lambda \, \Gamma(1-\eta) \times$$
$$\times \int_0^1 d\bar{x} \int_0^\infty d\omega \; \omega \left[m^2\omega^2 - 2\omega (p\cdot k_1 + \bar{x}\, p\cdot k_2) \right]^{-1+\eta} \qquad \text{(A2)}$$

$$V_\lambda^b = -2m^2 p_\lambda \, \Gamma(1-\eta) \times$$
$$\times \int_0^1 dz \int_0^\infty d\omega \; \omega \left[m^2\omega^2 - 2\omega (p\cdot k_1 + z\, p\cdot k_2) - k_2^2 z(1-z) \right]^{-1+\eta} \qquad \text{(A3)}$$

Each graph separately diverges at $\omega=\infty$, but the sum is finite (and actually zero for $k_2^2=0$). This is to be expected, as the contribution from (A1) satisfies a simple homogeneous Ward identity.

We are left with the contribution $V_\lambda^{b'}$ from graph (b) from the remainder of the 3-gluon vertex

$$-g_{\lambda\mu}(2k_2+k)_\nu + g_{\lambda\nu}(k_2-k)_\mu \qquad \text{(A4)}$$

This gives a numerator

$$-4 p_\lambda \, p\cdot(2k+k_2) \qquad \text{(A5)}$$

The ultraviolet divergent part of the integral is therefore proportional to

$$p_\lambda \int d^{4+2\eta} k \; (k^2+i\varepsilon)^{-1} \left[(k+k_2)^2 + i\varepsilon \right]^{-1} \qquad \text{(A6)}$$

The integral is a function of the single variable k_2^2. It may be renormalized in the usual minimum-subtraction way (temporarily

setting $\eta<0$), introducing a 't Hooft unit of mass μ. The result is proportional to

$$\eta^{-1} \left[(-k_2^2)^\eta - (\mu^2)^\eta \right]. \qquad \text{(A7)}$$

In order to obtain the form (4.7) for graphs containing (A7), we require formulae like

$$X^{-1+\eta} \, Y^{-1} = (1-\eta) \int_0^1 dz \; z^{-\eta} \left[Xz + Y(1-z) \right]^{-2+\eta} \qquad \text{(A8)}$$

The only complication is in z_k-dependence of $N_{\mu_1 \ldots \mu_r}$, which does not affect the ω-integral in (4.11).

Precisely similar remarks apply to gluon-vacuum-polarization and 3-gluon-vertex-part sub-graphs.

The only other complication is that, in a one-particle reducible graph, like (d) of Fig. 7, $\omega^{\sigma-1}$ in (4.11) must be replaced by $\omega^{\sigma-2}$.

APPENDIX B – MASS SINGULARITIES IN THE FEYNMAN GAUGE

In this Appendix, we first study how mass-singularities are produced in individual diagrams in the Feynman gauge, using the Feynman parameter form (4.11) of the eikonal integrals.

We begin with the specially simple case of just one real gluon. Then $C=0$ in (4.11) and the ω-integral can be done simply:

$$\Gamma(\nu-\ell\eta) \int_0^\infty d\omega \; \omega^{\sigma-1} \left(A\omega^2 + 2B\omega - i\varepsilon \right)^{-\nu+\ell\eta} = \qquad \text{(B1)}$$
$$= \Gamma(\sigma-\nu+\ell\eta) \, \Gamma(2\nu-\sigma-2\ell\eta) \, (2B-i\varepsilon)^{\sigma-2\nu+2\ell\eta} \, (A-i\varepsilon)^{\nu-\sigma-\ell\eta}$$

By the usual rules (pages 34, 35, 36 of [9]), A has the form

$$A = -sA_1(\bar{x}_i, \bar{y}_j, z_k) + m^2 \tag{B2}$$

where A_1 is bilinear in $\bar{x}_i$ and $\bar{y}_j$. With the notation

$$\bar{x}_i = u\hat{x}_i \quad , \quad \bar{y}_j = (1-u)\hat{y}_j \quad ,$$
$$\sum \hat{x}_i = \sum \hat{y}_j = 1, \tag{B3}$$

(B2) becomes

$$A = -s(1-u)u\,A_2(\hat{x}_i, \hat{y}_j, z_k) + m^2 \tag{B4}$$

Also, with this notation B has the structure

$$B = u\rho_\mu G^\mu(k_\alpha, \hat{x}_i, z_k) + (1-u)\rho'_\mu G^\mu(k_\alpha, y_j z_k) \tag{B5}$$

(Actually, in this case there is only one k_α, k_1).

Mass-singularities came from the regions $u = 0(m^2/s)$ and $1-u = 0(m^2/s)$. For definiteness, we take the former case.

The simplest example is when

$$\nu - \sigma = -1 \tag{B6}$$

and $B = 0(1)$. Then the u-integral of (B1) gives a term

$$O[(m^2)^{-\ell\eta}] \tag{B7}$$

On the other hand, the integral of $(2B-i\varepsilon)^{\sigma-2\nu+2\ell\eta}$ with respect to other variables may give terms

$$O[(up\cdot G)^{2\ell\eta}] \tag{B8}$$

and then the u-integration gives

$$O[(m^2)^{\ell\eta}] \tag{B9}$$

Another possibility is that $\nu-\sigma = 0$, but that the B-term gives

$$O[(up\cdot G)^{2\ell\eta-1}]$$

instead of (B8). Then the u-integration again gives (B9).

We have not found any examples in which the B-term produces $u^{\ell\eta}$ (instead of (B8)); but if it did, the u-integration would give $\ell n(s/m^2)$ instead of (B7) or (B9).

Next, we generalize to $C \neq 0$. We are concerned with A, given by (B4), being "small", or more strictly

$$|AC| \ll B^2 \tag{B10}$$

We may distinguish three cases:

(i) $$\sigma - 1 - \nu \leq -2 \tag{B11}$$

i.e, by (4.8)

$$\frac{1}{2}(n+\bar{n}-p-r) + \tau \leq -1 \tag{B12}$$

In this case, we get a convergent ω-integral by simply setting $A=0$ in (4.11). The corrections are $0(m^2)$, and there is no

mass-singularity. Note that (B12) requires at least two real gluons emitted from 3-gluon vertices, so $C \neq 0$.

(ii) $$\sigma - 1 - \nu \geq 0 \qquad \text{(B13)}$$

i.e.

$$\frac{1}{2}(n + \bar{n} - \gamma - r) + \zeta \geq 1 \qquad \text{(B14)}$$

In this case, the ω-integral would diverge if we just put $A=0$. Therefore, for small A, the mass-singularity comes from large ω. To estimate it, given (B10), we may set $C=0$, and still have a convergent integral at $\omega=0$. This therefore reduces to the case $C=0$, already studied in (B1), with the possible results (B7) and (B9).

(iii) $$\sigma - 1 - \nu = -1 \qquad \text{(B15)}$$

i.e.

$$\frac{1}{2}(n + \bar{n} - \gamma - r) + \zeta = 0 \qquad \text{(B16)}$$

Now, under condition (B10), there are important contributions both from small ω and from large ω. The contribution from large ω again has the approximate form (B1) (the only new feature being a coefficient $\Gamma(\ell\eta)$), with the results (B7) and (B9). The contribution from small ω is obtained by neglecting A, and is (using (B15))

$$\Gamma(\sigma)\,\Gamma(-\ell\eta)\,(2B - i\varepsilon)^{-\sigma}\,(C - i\varepsilon)^{\ell\eta} \qquad \text{(B17)}$$

This generates no mass-singularities. Its only role is to

cancel the pole at $\eta=0$ which appears in (B1) when (B15) holds.

Thus we conclude that (B7) and (B9) give the general mass-singularity behaviours.

A degenerate case of the above analysis occurs when all the gluons are attached to a single (anti-)quark line. Then $A_1 \equiv 0$ in (B2), and the mass-singularity is displayed in (B1) without doing any further integration.

The simplest example is afforded by the integrals in (A2) and (A3). These each have mass-singularities of the form (B7) (with $\ell=1$). The mass-singularity in (A3) can be found by neglecting k_2^2, in the manner of case (ii) above. Thus the singularities in (A2) and (A3) in fact cancel.

It is perhaps worth noticing that the cancellation between the mass-singularities in (A2) and (A3) is a consequence of the simple, homogeneous Ward identity obeyed by (A1). In this sense, the mass-singularity behaviour of (A2) and (A3) is a sort of model of the axial gauge behaviour predicted in Section 8 by the case of the Ward identity (8.9). Of course, the axial gauge is more complicated, because of the n-dependence of individual graphs. However, we argued in (8.7) that the n-dependence goes away in the complete set of relevant graphs.

The complete contribution to the vertex from (A4) also has mass-singularities ((A4) does not obey a simple Ward identity), which cancel with contributions from graphs involving both quark and antiquark line.

APPENDIX C - MASS SINGULARITIES IN MOMENTUM-SPACE

The appearance of mass-singularities like $m^{-2\ell\eta}$ in (B7) is a little surprising. It means that dimensional

regularization with $\eta>0$ does not regularize all the mass-singularities when $m=0$. It turns out that these singularities (as opposed to the $m^{2\ell\eta}$ ones) are a consequence of using the eikonal approximation and at the same time extending the momentum integrations to infinity. In this sense, these singularities in individual graphs are unphysical. Since, according to Section 8, the singularities cancel when all graphs are summed, their appearance in individual graphs does not invalidate the approximation (at least in the MNA sector). Presumably the approximation is saved by its gauge-invariance.

To elucidate these remarks, consider the simple example in Fig. 9.

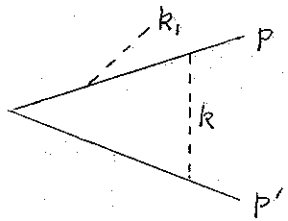

FIG. 9 – An example whose mass-singularities are studied in momentum space.

We complete the k_o-contour of integration in the lower half-plane, and display the contribution from the pole of the gluon-propagator (the contribution from the quark-propagator gives no mass-singularity).

In the centre-of-mass system, this gluon-pole term is (up to constants)

$$\frac{p_\lambda\, p_o\cdot p'}{p_o^3}\int d^{3+2\eta}\Omega\int_0^\infty dk\; k^{2+2\eta}\,(2k)^{-1}\,[-k(1+\beta x)]^{-1}\times$$

$$\times\,[k(1-\beta x)]^{-1}\,[k(1-\beta x)+p\cdot k_1\,(p_o)^{-1}]^{-1} \qquad (C1)$$

where

$$\frac{|\underset{\sim}{p}|}{p_o}=\frac{|\underset{\sim}{p}'|}{p_o'}=\beta$$

and

$$\hat{\underset{\sim}{p}}\cdot\hat{\underset{\sim}{k}}=-\hat{\underset{\sim}{p}}'\cdot\hat{\underset{\sim}{k}}=x$$

The k-integration in (C1) gives

$$\frac{p_\lambda\; p_o\cdot p'}{2p_o^3}\,\Gamma(\eta)\,\Gamma(1-2\eta)$$

$$\times\int d^{3+2\eta}\Omega\,(1+\beta x)^{-1}(1-\beta x)^{-1-2\eta}\left(\frac{p\cdot k_1}{p_o}\right)^{2\eta-1} \qquad (C2)$$

Since the angular integration $d^{3+2\eta}\Omega$ contains $(1-x^2)^\eta dx$ and since $4m^2=s(1-\beta^2)$, the region near $x=-1$ produces a mass-singularity proportional to

$$\frac{p_\lambda}{p\cdot k_1}\left(\frac{m\,p\cdot k_1}{s}\right)^{2\eta}, \qquad (C3)$$

and the region near $x=1$ produces

$$\frac{p_\lambda}{p\cdot k_1}\left(\frac{p\cdot k_1}{m}\right)^{2\eta} \qquad (C4)$$

The $m^{-2\eta}$ in (C4) is due to factor $(1-\beta x)^{-2\eta}$ in (C2), which is produced from the range of k-integration satisfying

$$k\gtrsim\frac{p_o k_1}{p_o}(1-\beta x)^{-1}\sim p\cdot k_1\,\frac{p_o}{m^2} \qquad (C5)$$

This range would have been excluded by a cut-off, for sufficiently small m^2.

These mass-singularities are ligaments of the eikonal approximation. This is illustrated by an exact calculation in which typically terms like

$$(m^2+2p\cdot k_1)^{-\eta}$$

occur. Such a term reduces to $(m)^{-2\eta}$ in the eikonal approximation.

APPENDIX D - MASS-SINGULARITIES IN THE AXIAL GAUGE

We first describe how Appendix C is modified in the axial gauge, defined by a unit, space-like vector n_μ. The on-shell gluon-propagator then introduces into (C1) an extra factor

$$\frac{1}{1+\beta^2}\,(n_0 k_0 - \underset{\sim}{n}\cdot\underset{\sim}{k})^{-2} \times$$

$$\times\left[(1-\beta^2)(k_T^2 n_0^2 + k_L^2 n_T^2) + k_T^2 - (1+\beta^2)(\underset{\sim}{k}_T\cdot\underset{\sim}{n}_T)^2 + \right. \tag{D1}$$

$$\left. + 2(\beta^2 n_0 k_0 - n_L\cdot k_L)\,\underset{\sim}{k}_T\cdot\underset{\sim}{n}_T\right]$$

where L and T denote component of 3-vectors parallel and perpendicular to $\underset{\sim}{p} = -\underset{\sim}{p}'$. In the case of (C1), the $\underset{\sim}{n}_T\cdot\underset{\sim}{k}_T$ term averages to produce a term proportional to k_T^2; so there is a suppression factor of either $(1-\beta^2)$ or

$$k_T^2 \;\propto\; (1-x^2) \tag{D2}$$

This has the consequence that (C2) has a smooth limit as $\beta\to 1$, the corrections being

$$O\left[(m^2)^{1-\eta}\right] \tag{D3}$$

This is in accord with the general expectations described in Section 8.

For gluons which are emitted and absorbed on the same quark line, however, the axial gauge does not have a similar

effect. It merely replaces the m^2 in the numerator (in, for example, (A2) and (A3)) by a factor proportional to $(1-x^2)$. In general, mass-singularities remain in individual graphs. We argued in Section 8 that these cancel out when a complete set of MNA graphs is summed.

Finally, we sketch a few details of an example designed to substantiate the claim in Section 8 that, even in the axial gauge, mass-singularities are unchanged when an external gluon goes off-shell. (An example of this example in the Feynman gauge is given by (A3)).

We take the example in Fig. 10.

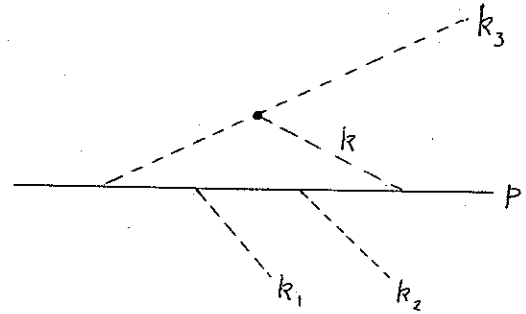

FIG. 10 - An example of an axial gauge graph designed to illustrate the independence of the mass singularity on the value of k_3^2.

Complete the contour in the lower half k_0-plane, and consider the contribution from the pole in $(k^2+i\varepsilon)^{-1}$. The relevant factors are then

$$\left[(2k\cdot k_3 + k_3^2)^{-1}\,(p\cdot k)^{-1}\,(p\cdot k + p\cdot k_2)^{-1} \times\right.$$

$$\left.\times\,(p\cdot k + p\cdot k_2 + p\cdot k_1)^{-1}\,k_\lambda\right]_{k_0 = |\underset{\sim}{k}|}\;|\underset{\sim}{k}|^{-1} \tag{D4}$$

Let $|\underset{\sim}{p}| = \beta p_o$ and $\hat{\underset{\sim}{k}}.\hat{\underset{\sim}{p}} = x$. For the most singular term near $x=1$, we may approximate k_λ by $|\underset{\sim}{k}|p_\lambda/p_o$ in the first and last term in the square bracket, to obtain

$$\frac{p_\lambda}{p_o}\left[2\,\frac{k(k_3.p)}{p_o} + k_3^2\right]^{-1}\left[k p_o\,(1-\beta x)\right]^{-1} \times$$

$$\times\left[k p_o(1-\beta x) + p.k_2\right]^{-1}\left[k p_o(1-\beta x) + p.k_2 + p.k_1\right]^{-1} \qquad \text{(D5)}$$

The k-integration now produces a factor

$$(1-\beta x)^{-2-2\eta} f(x) \qquad \text{(D6)}$$

where $f(x)$ is non-singular near $x = \beta^{-1}$.

We must supply a factor

$$(1-x^2) \qquad \text{(D7)}$$

from the axial-gauge propagator, but the angular integral of (D6) times (D7) still produces an $m^{-2\eta}$ mass-singularity.

The k_3^2 in the first denominator in (D5) only changes the behaviour of $f(x)$ away from $x = \beta^{-1}$, and so does not affect the mass-singularity. In fact the k_3^2-dependence is expected, just from eikonal-scaling, to be by terms of relative order

$$0\left[\,(m^2k_3^2/p.k_3) \times (\text{homogeneous function in } p.k_1 \text{ and } p.k_2 \text{ of degree } -1)\,\right] \qquad \text{(D8)}$$

There is a similar contribution from the other gluon pole $[(k+k_3)^2]^{-1}$. This is most easily evaluated by the change

of variables $k' = k+k_3$.

The reason for choosing the rather complicated example in Fig. 10 is that, in simpler cases, the contributions from the two gluon poles separately diverge at $k = \infty$ and have to be combined. When they are so combined, the conclusion is the same.

True ultraviolet divergences, in the axial gauge versions of Fig. 8, cancel by the simple Ward identity in the same sort of way as in (A2) and (A3).

ACKNOWLEDGEMENTS

One of us (J.C.T.) is grateful to Conselho Nacional de Pesquisas (CNPq) and Fundação de Amparo à Pesquisa do Estado de São Paulo (FAPESP) for financial support and to Instituto de Física da Universidade de São Paulo for the hospitality extended to him.

Another (J.G.M.G.) acknowledges receipt of a studentship from S.E.R.C. J. Frenkel acknowledges a grant from CNPq.

We thank D.E. Soper and C.T. Sachrajda for useful conversations.

REFERENCES

[1] J. Frenkel, M.J. Shailer and J.C. Taylor, Nucl. Phys. B148, 228 (1979); G. Altarelli, R.K. Ellis and G. Martinelli, Nucl. Phys. B157, 461 (1974); R.K. Ellis, H. Georgi, M. Machacek, H.D. Politzer and G.G. Ross, Nucl. Phys. B152, 285 (1979).

[2] G.T. Bodwin, S.J. Brodsky and G.P. Lepage, Phys. Rev. Lett. 47, 1799 (1981).

[3] W.W. Lindsay, D.A. Ross and C.T. Sachrajda, Phys. Lett. 117B, 105 (1982) and Southampton preprint.

[4] R. Doria, J. Frenkel and J.C. Taylor, Nucl. Phys. B168, 93 (1980); A. Andrasi, M. Day, R. Doria, J. Frenkel and J.C. Taylor, Nucl. Phys. B182, 104 (1981); C. Di Lieto, S. Gendron, I.G. Halliday and C.T. Sachrajda, Nucl. Phys. B183, 223 (1981); J. Frenkel, J.G.M. Gatheral and J.C. Taylor "Soft gluons and the eikonal approximation with massless quarks", Nucl. Phys. (to be published).

[5] J.G.M. Gatheral, "Exponentiation of eikonal cross sections in nonabelian gauge theories" (Cambridge preprint DAMTP 83/3).

[6] T. Appelquist and J. Carazzone, Nucl. Phys. B120, 77 (1977).

[7] H. Banerjee, M. Sengupta and A. Chattergee, "Failure of Bloch-Nordsieck mechanism in perturbative QCD", CERN preprint TH 3544 (1983).

[8] S.B. Libby and G. Sterman, Phys. Rev. D19, 2468 (1979).

[9] R.J. Eden, P.V. Landshoff, D.I. Olive and J.C. Polkinghorne, "The analytic S-matrix" (Cambridge University Press, 1966).